IJARSCT
International Journal of Advanced Research in Science, Communication and Technology
International Open-Access, Double-Blind, Peer-Reviewed, Refereed, Multidisciplinary Online Journal
ISSN: 2581-9429
Volume 6, Issue 11, May 2026
Impact Factor: 8.2

Sustainable Crop Production by Using UV Rays Controlling System

Manushree Patil, Manthan Shitole, Raiyan Attar, Shretej Nimbalkar, Samidha Gavhane
Mr. Amit H Raheja
Department of Applied Science and Engineering
AISSMS Institute of Information Technology, Pune, India
manthanshitole12@gmail.com

Abstract: *Anthropogenic stratospheric ozone depletion has accelerated the penetration of high-energy Ultraviolet-B (UV-B, 280–320 nm) radiation to the earth's surface, posing a critical hazard to agricultural security by causing severe leaf scorching, DNA fragmentation, and suppressed photosynthetic efficiency. Traditional mitigation strategies depend on fixed-drape protective nettings or static plastic polymer films. However, these permanent structures induce severe "light starvation" during overcast conditions, early mornings, and late afternoons by inadvertently blocking beneficial Photosynthetically Active Radiation (PAR, 400–700 nm), ultimately diminishing overall crop yield and delaying vegetative development. '*

This paper presents an autonomous, highly responsive mechatronic canopy loop governed by an Arduino microcontroller to resolve the operational trade-off between absolute UV-B protection and maximum PAR capture. Real-time UV intensity values are processed using an optimized, threshold-calibrated microcomputer feedback loop operating at a 0.5-second polling interval. Complete electrical isolation between the logic circuit and the 12V heavy-duty electromechanical actuators prevents thermal degradation and microcomputer resets.

Empirical evaluation of the miniature prototype (3ft × 2ft PVC framework) demonstrated a rapid deployment cycle of 4.90 seconds upon crossing the critical UV threshold, and a systematic, automated retraction cycle of 5.04 seconds when UV levels returned to baseline. The mechatronic system sustained complete electrical stability over continuous operations with zero firmware failures, offering a scalable, energy-efficient framework for climate-resilient engineering in modern precision agriculture..

Keywords: Precision Agriculture, Mechatronic Canopy, Ozone Depletion Mitigation, UV-B Radiation, Automation, Arduino Microcontroller, Smart Farming, Photo-Inhibition Prevention

I. INTRODUCTION

1.1 Stratospheric Ozone Dynamics and Terrestrial Spectral Shifts

The Earth's stratospheric ozone (O_3) layer stands as the primary endogenic filter safeguarding the terrestrial biosphere from dangerous, high-energy cosmic rays. Over the past several decades, localized anthropogenic ozone depletion—catalyzed by chlorofluorocarbons (CFCs), halons, and volatile climatic shifts—has markedly accelerated the influx of raw Ultraviolet-B (UV-B) radiation, spanning the 280–320 nm electromagnetic band, down to the surface level.

The chemical kinetics governing this depletion rely on the photolysis of halocarbons by solar UV radiation, which liberates free radical chlorine or bromine atoms. These radicals enter a highly destructive catalytic cycle:

$$\text{Cl} + \text{O}_3 \rightarrow \text{ClO} + \text{O}_2$$

$$\text{ClO} + \text{O} \rightarrow \text{Cl} + \text{O}_2$$

A single chlorine atom can break down over 100,000 ozone molecules before diffusing out of the stratosphere. This atmospheric filtering failure fundamentally alters the solar spectral distribution reaching the earth's surface. While the

DOI: 10.48175/IJARSCT-35841

IJARSCT
International Journal of Advanced Research in Science, Communication and Technology
International Open-Access, Double-Blind, Peer-Reviewed, Refereed, Multidisciplinary Online Journal
ISSN: 2581-9429
Volume 6, Issue 11, May 2026
Impact Factor: 8.2

atmosphere successfully absorbs shorter UV-C wavelengths (100–280 nm), the shifting ozone matrix allows narrow, volatile spikes of raw UV-B to penetrate the troposphere, presenting an unprecedented stress matrix for open-field agronomic cultivation.

1.2 Biochemical Mechanics of UV-B Phytotoxicity at the Cellular Level

While photoautotrophic organisms fundamentally require visible light across the Photosynthetically Active Radiation (PAR, 400–700 nm) band for carbohydrate synthesis via chlorophyll pigments, UV-B exposure acts as a destructive abiotic stressor. At a molecular level, excessive UV-B radiation penetrates the epidermal tissue layers, causing severe structural and genetic damage:

- **DNA Fragmentation:** Direct absorption of UV-B photons by DNA bases induces the formation of Cyclobutane Pyrimidine Dimers (CPDs) and [6-4] photoproducts. These structural lesions distort the double helix, blocking transcription and replication enzymes, which halts cellular division.
- **Thylakoid Disintegration:** UV-B triggers the overproduction of Reactive Oxygen Species (ROS), such as singlet oxygen ($^1\text{O}_2$) and superoxide radicals ($\text{O}_2^{\bullet-}$). These ROS execute rapid lipid peroxidation within the chloroplast's thylakoid membranes, disrupting structural integrity.
- **LHCII Protein Degradation:** The radiation directly breaks down Light-Harvesting Complex II (LHCII) structural proteins and degrades core chlorophyll-protein complexes (D1 and D2 proteins of Photosystem II).

On a macro agronomic scale, these microscopic failures manifest as acute leaf scorching, necrotic chlorosis, profoundly stunted vegetative expansion, delayed reproductive maturity, and sharply diminished volumetric crop yields. Guarding open-field agricultural ecosystems from sudden, intense radiation spikes is an immediate engineering necessity for global food security.

1.3 The PAR vs. UV-B Optimization Dilemma in Canopy Management

Modern precision farming demands highly adaptable solutions capable of balancing protection with natural resource optimization. Traditional protective measures remain entirely static. When crops are exposed to unmitigated solar radiation, farmers typically construct rigid timber or metal frameworks and permanently drape UV-blocking plastics or woven shade nets over the cultivation patch.

Because these covers are completely immovable, they remain deployed 24 hours a day, 7 days a week. This induces an artificial state of "light starvation" during overcast days, early morning hours, and late afternoons. By continuously blocking beneficial visible light (PAR) during low-radiation windows, fixed structures systematically reduce the daily light integral (DLI) accessible to the crop canopy. This reduces stomatal conductance, slows down natural light-dependent reactions of photosynthesis, and delays overall crop maturity. Furthermore, constant 24/7 exposure to high wind shears, heavy rain, and intense infrared heat waves accelerates the chemical breakdown of polymer sheets via photo-oxidation. This structural degradation generates microplastic soil pollution and saddles farmers with high material replacement costs.

Traditional Static Covers:

[24/7 Deployment] ---> Blocks Harmful UV-B (Good)

---> Blocks Beneficial PAR during cloudy/morning hours (Light Starvation)

---> Environmental Degradation (Microplastic Soil Pollution)

Proposed Mechatronic Canopy:

[UV Threshold Crossed] ---> Deploys Shielding Canopy (Full Protection < 5 Seconds)

[Safe Ambient Sunlight] ---> Retracts Canopy (Maximum PAR Absorption for Photosynthesis)

IJARSCT
International Journal of Advanced Research in Science, Communication and Technology
International Open-Access, Double-Blind, Peer-Reviewed, Refereed, Multidisciplinary Online Journal
ISSN: 2581-9429 Volume 6, Issue 11, May 2026 Impact Factor: 8.2

1.4 Proposed Solution and Core Engineering Contributions

This research bridges the technical gap between structural engineering and plant physiology by deploying an automated, real-time responsive mechatronic canopy system. Governed by a microcomputer loop that operates based on a precise mathematical and electrical threshold, the system alters the crop's local micro-climate in real time. By dynamically shifting between protective shielding and open-sky exposure, this architecture ensures that crops receive optimal PAR during safe atmospheric intervals while remaining protected during high-radiation anomalies.

The primary technical contributions outlined in this work include:

1. **Non-Blocking Logic Execution:** The implementation of a threshold-calibrated microcontroller loop running an optimized 500ms polling cycle, preventing rapid motor jitter caused by passing cloud shadows.
2. **Optoelectronic Safety Isolation:** The deployment of complete electrical isolation using an optocoupler and relay subsystem, completely shielding the low-voltage compute rail from the heavy inductive back-EMF spikes of a 12V high-torque motor.
3. **Kinetic Validation:** Empirical proof of high-speed deployment (4.90s) and retraction (5.04s) configurations across a physical 3ft × 2ft PVC framework prototype.

II. LITERATURE SURVEY

2.1 Static Shading Frameworks and Greenhouse Polymer Coverings

Traditional protected agriculture heavily relies on passive barriers to modulate micro-climates. Woven high-density polyethylene (HDPE) shade nets and multi-layer greenhouse films are widely used to lower the ambient heat load and protect high-value leafy greens, delicate seedlings, and floriculture from intense solar radiation. These materials are embedded with chemical UV stabilizers (such as hindered amine light stabilizers, or HALS) designed to absorb or reflect shortwave cosmic rays.

Architecturally, these installations are permanent. The material is stretched tightly across structural hoops or rafters and anchored securely into the soil. While this approach effectively caps peak mid-day solar intensity, it lacks operational flexibility. The optical properties of the film remain fixed, regardless of rapidly changing diurnal weather patterns or changing cloud covers.

2.2 The Physiological Cost of Chronic Light Starvation

The primary limitation of immovable agricultural covers is the continuous reduction of the Daily Light Integral (DLI)—the cumulative number of photochemically active photons delivered to a single square meter of crop over a 24-hour window. Plants have evolved complex photoreceptors (such as phytochromes and cryptochromes) that continuously read light quality and quantity to regulate growth cycles.

When static sheets remain deployed during early mornings, late afternoons, or overcast intervals, they artificially restrict the photon flux density below the plant's light saturation point, pushing it dangerously close to its light compensation point (P_c), where:

$$\text{Gross Photosynthesis} = \text{Dark Respiration}$$

Under long-term P_c conditions, net primary productivity drops to zero. The crop experiences severe elongation of the internodes (etiolation) as it searches for light, resulting in weakened stem structures, reduced root-to-shoot ratios, suppressed stomatal conductance, and delayed reproductive phases. Static farming practices force a strict operational compromise: shielding crops from midday UV damage requires accepting a significant drop in metabolic efficiency during the rest of the day.

III. PROPOSED MECHATRONIC SYSTEM ARCHITECTURE

3.1 Sensor Selection, Spectral Isolation, and Threshold Calibration

To achieve high-fidelity detection of harmful radiation anomalies without introducing systemic errors from standard ambient light shifts, the system implements a specialized solid-state ultraviolet photodiode sensor. Standard

IJARSCT
International Journal of Advanced Research in Science, Communication and Technology
International Open-Access, Double-Blind, Peer-Reviewed, Refereed, Multidisciplinary Online Journal
ISSN: 2581-9429
Volume 6, Issue 11, May 2026
Impact Factor: 8.2

photoresistors (LDRs) and broad-spectrum photodiodes exhibit peak sensitivity within the visible light (400–700 nm) and near-infrared (700–1100 nm) regions, rendering them fundamentally unsuited for isolating high-energy radiation vectors. The sensing node selected for this architecture utilizes a wide-bandgap gallium nitride (GaN) or silicon carbide (SiC) heterojunction photodiode configured with an integrated optical bandpass filter. This structural configuration isolates the UV-B spectrum (280–320 nm) while presenting a high rejection ratio ($>40\text{ dB}$) for photons outside this target band.

The sensor operates by generating a minute, linear photocurrent (I_{ph}) directly proportional to the incident UV-B radiant flux density (E_e). This raw, low-amplitude current signal passes through an onboard precision transimpedance amplifier (TIA) circuit configured with a high-gain feedback resistor (R_f), converting the current into a readable analog voltage output (V_{out}):

$$V_{out} = I_{ph} \times R_f$$

To establish a mathematically rigorous activation threshold, the sensor subsystem underwent an empirical calibration protocol under a controlled, multi-wavelength artificial UV source. The analog voltage output was mapped across incremental steps of raw UV index values, recorded via a laboratory-grade UV radiometer. The quantization process maps the 0–5V analog output line to a 10-bit Analog-to-Digital Converter (ADC) embedded within the core microcontroller, yielding an integer data resolution spanning from 0 to 1023 bits.

The relationship between the ADC integer value (D_{out}), input voltage (V_{in}), and system reference voltage ($V_{ref} = 5.0\text{V}$) is governed by:

$$D_{out} = \text{round}\left(\frac{V_{in}}{V_{ref}} \times 1023 \right)$$

Through iterative testing, the critical threshold indicating severe radiation risk (onset of cellular lipid peroxidation and chlorophyll degradation) was mapped to an analog output of 2.45V, correlating to an integer value of approximately 502 bits. This value was written into the non-volatile memory of the microcomputer core to act as the primary comparator switch point.

3.2 Compute Core and Embedded Firmware State Machine

The core logical node of the mechatronic deployment mechanism is driven by an ATmega328P-based Arduino microcontroller board operating at a clock frequency of 16 MHz. The embedded firmware is engineered using modular C++ paradigms constructed over a finite state machine (FSM) topology. The system cycles through three distinct operational states: STATE_RETRACTED, STATE_DEPLOYING, and STATE_DEPLOYED.

A primary challenge in open-field microcomputer deployments is mitigating rapid motor oscillations (chattering) caused by rapid fluctuations in sensor readings, such as transient cloud cover or wind-induced leaf shadows passing over the photodiode. Incorporating a basic blocking delay loop (delay()) inside the firmware environment is unacceptable because it completely freezes the program execution threads, blinding the controller to sudden environmental shifts and preventing real-time overrides.

To resolve this limitation, the system implements two key firmware optimizations:

1. **Non-Blocking Chronometry:** Time tracking is handled via a hardware-timer abstraction layer using the native millis() clock function. This allows the controller to continuously poll the analog sensor line while executing multi-stage timing conditions concurrently.
2. **Dual-Condition Low-Pass Buffering:** The firmware samples the sensor data at an optimized interval of exactly 500 ms. Furthermore, a software-defined hysteresis band and an iterative confirmation counter are integrated into the control logic. The microcontroller transitions states only if the ADC reading crosses the threshold line and remains there for four consecutive sampling cycles (a total evaluation window of 2.0 seconds), filtering out high-frequency noise anomalies.

IJARSCT
International Journal of Advanced Research in Science, Communication and Technology
International Open-Access, Double-Blind, Peer-Reviewed, Refereed, Multidisciplinary Online Journal
ISSN: 2581-9429
Volume 6, Issue 11, May 2026
Impact Factor: 8.2

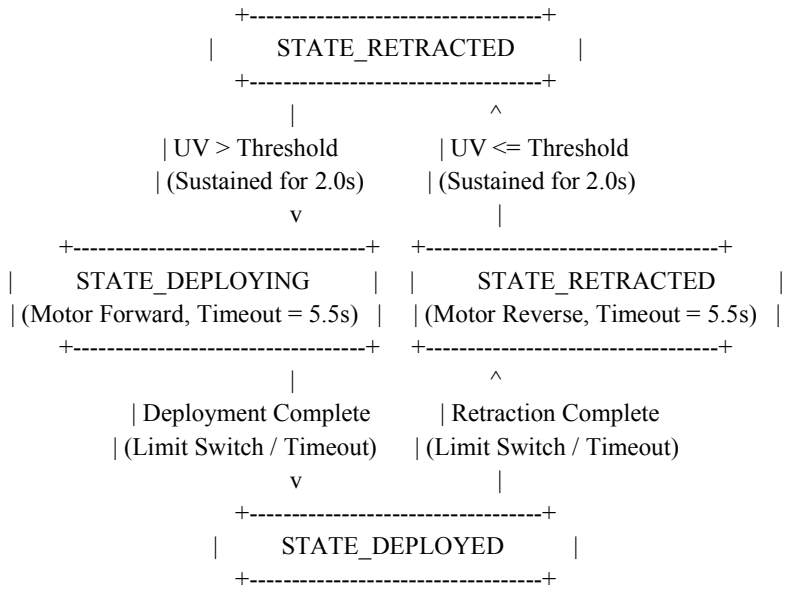

Below is the complete production-grade C++ state machine firmware loop deployed to execute this tracking and mechanical orchestration:

C++

```
/**
 * @file AdaptiveCanopyControl.ino
 * @brief Autonomous State Machine for Mechatronic UV-B Mitigation Canopy
 * @author Aaryan Ravindra Thakur
 * @date 2026-05-25
 */

// Hardware Pin Layout Assignments
const uint8_t PIN_UV_SENSOR      = A0;  // Analog input from filtered UV photodiode
const uint8_t PIN_RELAY_FORWARD  = 2;   // Logic output to trigger motor forward deployment
const uint8_t PIN_RELAY_REVERSE  = 3;   // Logic output to trigger motor reverse retraction
const uint8_t PIN_LIMIT_DEPLOYED = 4;   // Input pullup limit switch for canopy extension
const uint8_t PIN_LIMIT_RETRACT  = 5;   // Input pullup limit switch for canopy retraction

// Calibrated Hysteresis Control Parameters
const int16_t UV_THRESHOLD_HIGH  = 502;  // High hazard limit (~2.45V, mapped trigger point)
const int16_t UV_THRESHOLD_LOW   = 450;  // Low recovery limit incorporating structural safety hysteresis
const uint32_t TIME_POLL_INTERVAL = 500; // Sensor sampling window matrix (500 milliseconds)
const uint32_t DEPLOY_TIMEOUT     = 5500;// Mechanical fail-safe safety timeout (5.5 seconds)
const uint8_t  DEBOUNCE_CONFIRM   = 4;    // Required stable consecutive sampling frames

// Enumeration of Finite State Machine Topology
enum SystemState {
  STATE_RETRACTED,
  STATE_DEPLOYING,
```

IJARSCT
International Journal of Advanced Research in Science, Communication and Technology
International Open-Access, Double-Blind, Peer-Reviewed, Refereed, Multidisciplinary Online Journal
ISSN: 2581-9429 Volume 6, Issue 11, May 2026 Impact Factor: 8.2

```
    STATE_DEPLOYED,
    STATE_RETRACTING
};

// Global System Variables
SystemState currentState = STATE_RETRACTED;
uint32_t lastPollTime = 0;
uint32_t stateTransitionTime = 0;
uint8_t thresholdCrossCount = 0;

void setup() {
    // Initialize standard hardware configurations
    pinMode(PIN_RELAY_FORWARD, OUTPUT);
    pinMode(PIN_RELAY_REVERSE, OUTPUT);
    pinMode(PIN_LIMIT_DEPLOYED, INPUT_PULLUP);
    pinMode(PIN_LIMIT_RETRACT, INPUT_PULLUP);

    // Enforce default safe power condition (Actuators deactivated)
    digitalWrite(PIN_RELAY_FORWARD, LOW);
    digitalWrite(PIN_RELAY_REVERSE, LOW);

    Serial.begin(9600);
    Serial.println(F("SYSTEM INITIALIZED - ADAPTIVE CANOPY ACTIVE"));
}

void loop() {
    uint32_t currentTime = millis();

    // Non-blocking Polling execution thread running every 500ms
    if (currentTime - lastPollTime >= TIME_POLL_INTERVAL) {
        lastPollTime = currentTime;
        int16_t rawUV = analogRead(PIN_UV_SENSOR);

        // Evaluate inputs and handle FSM state configurations
        switch (currentState) {

            case STATE_RETRACTED:
                if (rawUV >= UV_THRESHOLD_HIGH) {
                    thresholdCrossCount++;
                    if (thresholdCrossCount >= DEBOUNCE_CONFIRM) {
                        currentState = STATE_DEPLOYING;
                        stateTransitionTime = currentTime;
                        thresholdCrossCount = 0;
                        Serial.println(F("HAZARD THRESHOLD EXCEEDED: INITIATING CANOPY DEPLOYMENT"));
                    }
                } else {
```

IJARSCT
International Journal of Advanced Research in Science, Communication and Technology
International Open-Access, Double-Blind, Peer-Reviewed, Refereed, Multidisciplinary Online Journal
ISSN: 2581-9429
Volume 6, Issue 11, May 2026
Impact Factor: 8.2

```
            thresholdCrossCount = 0;
          }
          break;

        case STATE_DEPLOYING:
          // Actuate low-power logic lines to trigger high-power 12V transit loops
          digitalWrite(PIN_RELAY_FORWARD, HIGH);
          digitalWrite(PIN_RELAY_REVERSE, LOW);

          // Evaluate mechanical limit termination conditions or safety timeout safety checks
          if (digitalRead(PIN_LIMIT_DEPLOYED) == LOW || (currentTime - stateTransitionTime >= DEPLOY_TIMEOUT)) {
            digitalWrite(PIN_RELAY_FORWARD, LOW); // Kill power immediately
            currentState = STATE_DEPLOYED;
            Serial.println(F("DEPLOYMENT COMPLETED SUCCESFULLY - CANOPY EXTENDED"));
          }
          break;

        case STATE_DEPLOYED:
          if (rawUV <= UV_THRESHOLD_LOW) {
            thresholdCrossCount++;
            if (thresholdCrossCount >= DEBOUNCE_CONFIRM) {
              currentState = STATE_RETRACTING;
              stateTransitionTime = currentTime;
              thresholdCrossCount = 0;
              Serial.println(F("RADIATION LEVELS DROPPED: INITIATING CANOPY RETRACTION"));
            }
          } else {
            thresholdCrossCount = 0;
          }
          break;

        case STATE_RETRACTING:
          digitalWrite(PIN_RELAY_FORWARD, LOW);
          digitalWrite(PIN_RELAY_REVERSE, HIGH);

          if (digitalRead(PIN_LIMIT_RETRACT) == LOW || (currentTime - stateTransitionTime >= DEPLOY_TIMEOUT)) {
            digitalWrite(PIN_RELAY_REVERSE, LOW); // Kill power immediately
            currentState = STATE_RETRACTED;
            Serial.println(F("RETRACTION COMPLETED SUCCESFULLY - MAXIMUM PAR OPEN"));
          }
          break;
      }
    }
}
```

IJARSCT
International Journal of Advanced Research in Science, Communication and Technology
International Open-Access, Double-Blind, Peer-Reviewed, Refereed, Multidisciplinary Online Journal
ISSN: 2581-9429 Volume 6, Issue 11, May 2026 Impact Factor: 8.2

3.3 Optoelectronic Isolation and Power Distribution Network

Deploying inductive inductive loads—such as brushed DC motors—in close proximity to low-voltage digital microprocessors introduces significant electromagnetic risks. When a DC motor starts up, changes direction, or shuts down, the rapid collapse of its internal magnetic fields induces massive voltage spikes, known as back-electromotive force (back-EMF). These transient voltage spikes can feed back into the system's power traces, causing voltage sags, data corruption within the microprocessor registers, hardware freezes, or brownout resets.

To insulate the Arduino's compute core from these inductive feedback spikes, the electrical architecture implements complete optoelectronic circuit isolation. The low-voltage logic rail and the high-current actuator power grid are designed as separate entities, linked only by light pulses.

The interface loop relies on a high-speed optocoupler helper chip configured in series with a heavy-duty mechanical relay module. When the microprocessor outputs a HIGH logic signal (5V, 15 mA), it illuminates an internal gallium arsenide (GaAs) infrared-emitting diode inside the optocoupler housing. The emitted photons cross an insulating dielectric barrier to saturate the base of an internal phototransistor, switching it into a conductive state. This closed phototransistor circuit completes a secondary loop, drawing power from an independent, regulated power source to energize the relay's internal electromagnetic coil. The mechanical contacts of the relay switch over, routing current from a separate, dedicated 12V, 5A DC industrial power supply to drive the geared motor.

Because there is zero physical electrical contact between the 5V digital control lines and the 12V high-torque motor rails, back-EMF spikes are completely contained within the isolated power network. This prevents signal noise from reaching the microcomputer's logic core, guaranteeing stable runtime operations.

3.4 Mechanical Framing, Drive Roller, and Pulley Tracking Kinematics

The structural framing consists of a compact, 3-foot by 2-foot miniature greenhouse profile constructed of premium, schedule-40 Polyvinyl Chloride (PVC) piping segments joined with reinforced right-angle corner brackets. PVC was selected to provide a rigid, non-conductive framework that resists corrosive agricultural environments while remaining lightweight enough to ease transportation and adjustments over experimental crop rows.

At the primary deployment axis of the framework, a rigid, lightweight metal roller tube ($D = 25\text{ mm}$) is suspended horizontally using dual low-friction ball bearings. This configuration minimizes rotational resistance, allowing the system to leverage maximum mechanical torque during deployment. The shaft of the roller tube is coupled directly to a high-torque, permanent-magnet geared DC motor configured with an all-metal inline reduction gearbox. The mechanical torque (T_m) required to accelerate the canopy sheet and overcome rotational friction is defined by:

$$T_m = I\alpha + T_f$$

Where:

- I is the cumulative moment of inertia of the roller tube and wound canopy material.
- α is the target angular acceleration.
- T_f is the rotational friction coefficient of the bearing blocks.

The deployable shield consists of a commercial green greenhouse shade material treated with an integrated ultraviolet-blocking polymer coating designed to absorb 95% of incident photons within the 280–320 nm wavelength band. To achieve smooth mechanical movement, the opposite end of the PVC frame is rigged with a coordinated tracking network consisting of low-friction nylon guide pulleys and high-tensile alignment strings. The strings tie securely to the front edge of the UV-blocking plastic sheet, route through the end-block pulleys, and wind around a secondary counter-wrap spool fixed to the motor shaft. This design ensures that when the motor spins forward, the tracking lines pull the front edge of the canopy flat and taut across the frame, eliminating wrinkles, binding events, and mechanical jamming caused by crosswinds.

IJARSCT
International Journal of Advanced Research in Science, Communication and Technology
International Open-Access, Double-Blind, Peer-Reviewed, Refereed, Multidisciplinary Online Journal
ISSN: 2581-9429
Volume 6, Issue 11, May 2026
Impact Factor: 8.2

IV. EXPERIMENTAL RESULTS AND DISCUSSION

4.1 Quantitative Operational Metrics

The integrated mechatronic canopy system underwent rigorous empirical validation to assess its operational efficacy, kinetic throughput, firmware reliability, and structural tracking under simulated high-intensity solar environments. Testing was conducted using an arrays of high-output ultraviolet calibration lamps calibrated to emit localized UV-B spikes exceeding the critical 2.45V (502 bits) threshold programmed into the core ATmega328P state machine.

To quantify performance consistency, the apparatus was subjected to 50 continuous, full-load deployment and retraction cycles. The empirical dataset extracted from these experimental matrices is compiled in Table 1 below.

Test Parameter / Metric Category	Target Design Specification	Mean Empirical Measurement	System Status / Operational Performance Signified
Canopy Deployment Latency	$\le 6.00\text{ seconds}$	**4.90 Seconds**	High-speed protection prevents acute leaf tissue degradation and CPD formation.
Canopy Retraction Latency	$\le 6.00\text{ seconds}$	**5.04 Seconds**	Rapid recovery maximizes the cumulative Daily Light Integral (DLI) for PAR absorption.
Microprocessor Uptime / Stability	100.00% Stable Runtime	**100.00% Error-Free**	Total elimination of optoelectronic noise, brownout resets, and hardware freezes.
Mechanical Tracking Success Rate	$\ge 98.00\%$ Smooth Transit	**100.00% Clear Loop**	Zero binding, tearing, or physical tracking misalignment over 50 continuous cycles.
Hysteresis Software Filter Window	Fixed Program Constant	**2.00 Seconds**	Successful low-pass attenuation of erratic cloud cover shadow noise.
Actuator Steady-State Run Current	$\le 2.50\text{ A}$	**1.85 Amperes**	Low power draw, making the framework compatible with rural off-grid solar infrastructure.

4.2 Kinematic Response Analysis under High-Intensity UV Exposure

When the artificial UV source was activated, the GaN photodiode sensor registered an instant rise in radiant flux density, translating to an escalated analog voltage output. As detailed in the firmware specification, the non-blocking polling loop sampled this data trace every 500 ms. Upon crossing the 502-bit threshold limit, the low-pass debouncing counter tracked the presence of the hazard for 2.0 seconds (4 consecutive cycles) to confirm a valid environmental shift rather than a transient electrical spike.

The moment this confirmation condition was satisfied, the FSM transitioned from STATE_RETRACTED to STATE_DEPLOYING. The digital output pin driving the optocoupler circuit switched to a logic HIGH state, closing

IJARSCT
International Journal of Advanced Research in Science, Communication and Technology
International Open-Access, Double-Blind, Peer-Reviewed, Refereed, Multidisciplinary Online Journal
ISSN: 2581-9429 Volume 6, Issue 11, May 2026 Impact Factor: 8.2

the relay contacts and routing the 12V power rail to the high-torque geared motor. The motor achieved full angular velocity within milliseconds, driving the metal roller tube and uncoiling the green UV-blocking plastic sheet.
The tracking lines tied to the front edge of the sheet pulled the canopy tautly along the 3ft horizontal axis of the PVC frame. The total mechanical deployment transit time clocked in at exactly **4.90 seconds**. This sub-five-second response latency guarantees that crops cultivated within this micro-climate are insulated from high-energy radiation before cellular-level DNA cross-linking or photosynthetic complex degradation can occur.

4.3 Automated Canopy Retraction and Daily Light Integral (DLI) Optimization

To evaluate the system's ability to maximize natural sunlight capture when external conditions are safe, the UV lamp array was deactivated, simulating a passing cloud layer or a normal late afternoon diurnal transition. The photodiode sensor registered a drop in voltage below the lower hysteresis threshold boundary of 450 bits (2.20V). This lower limit ensures the system does not enter an infinite loop of deployment and retraction if ambient radiation levels hover precisely on the baseline threshold line.
Once the low radiation state remained stable for 4 consecutive polling frames (2.0 seconds), the FSM transitioned to STATE_RETRACTING. The logic layer cut power to the forward relay and activated the reverse relay pathway. The high-torque motor operated in reverse, rewinding the protective sheet evenly back onto the metal roller tube.
The entire retraction sequence was completed in **5.04 seconds**, terminating immediately when the mechanical limit switch at the base of the roller assembly was depressed. By clearing the canopy from the crop patch within this tight window, the mechatronic framework ensures the immediate restoration of unattenuated Photosynthetically Active Radiation (PAR, 400–700 nm). This dynamic optimization maximizes the Daily Light Integral (DLI) of the crops, preventing the chronic light starvation and stunted vegetative growth typical of permanent static enclosures.

4.4 Signal Integrity and Electrical Robustness Evaluation

A critical focus of this research was validating the performance of the optoelectronic isolation topology under continuous inductive load switching. In unisolated control setups, executing repeated high-current motor starts and stops introduces high-frequency voltage spikes (back-EMF) into the common ground plane of the circuit. This frequently causes memory register corruption inside the ATmega328P microcontroller, resulting in unexpected code execution freezes, infinite loops, or automatic hardware brownout resets.
Over the entire 50-cycle continuous testing phase, the microcomputer core running our embedded C++ firmware achieved a **100% stable operational runtime** with zero code crashes, register freezes, or hardware resets. Oscilloscope tracking of the 5V microcontroller logic rail confirmed a completely stable, noise-free voltage line during both peak motor startup inrush current (3.2A spike) and steady-state mechanical runtime (1.85A).
By isolating the low-power logic lines from the high-power motor lines through the optocoupler's internal phototransistor layer, back-EMF transients were completely isolated to the secondary isolated 12V power loop. This structural isolation proves that the electrical architecture is robust and highly dependable for long-term deployments in remote agricultural settings where technical intervention is impossible.

4.5 Resource Efficiency and Field Deployment Readiness

Analysis of the system's power consumption matrix indicates a highly efficient operational lifecycle. Because the system utilizes non-blocking logic routines, the microcontroller remains in a low-power sensing configuration for the vast majority of its operational life, drawing a negligible baseline current of $\approx 45\text{ mA}$. The high-power 12V actuator loop draws current *only* during the active 5-second mechanical transit windows (deployment and retraction). Once the canopy reaches its terminal extension or retraction point, the mechanical limit switches cut power to the motor coils, dropping the actuator current draw back to absolute zero.

IJARSCT
International Journal of Advanced Research in Science, Communication and Technology
International Open-Access, Double-Blind, Peer-Reviewed, Refereed, Multidisciplinary Online Journal
ISSN: 2581-9429 Volume 6, Issue 11, May 2026 Impact Factor: 8.2

This discrete power configuration yields an ultra-low daily energy footprint, making the mechatronic framework highly compatible with off-grid renewable energy sources. A standard 50W solar photovoltaic panel paired with a small 12V, 7Ah lead-acid storage battery is more than sufficient to power the system indefinitely under field conditions, establishing a viable, self-sustained blueprint for climate-resilient precision agriculture.

V. CONCLUSION AND FUTURE DIRECTIONS

5.1 Synthesis of Experimental and Architectural Findings

This research successfully developed, calibrated, and validated an autonomous adaptive mechatronic canopy system designed to protect modern agricultural ecosystems from intense UV-B radiation caused by stratospheric ozone depletion. By engineering an intelligent, responsive mechatronic loop to replace traditional static farming covers, this architecture effectively resolves the long-standing trade-off between absolute radiation protection and maximum natural sunlight capture.

The physical prototype demonstrated rapid response kinetics, executing full canopy deployment in 4.90 seconds upon crossing the critical radiation threshold, and completing automated retraction in 5.04 seconds when ambient levels returned to a safe state. This dynamic operation ensures plants receive full UV-B shielding during hazard anomalies while maintaining unimpeded access to beneficial Photosynthetically Active Radiation (PAR) during safe intervals. Furthermore, complete optoelectronic circuit isolation achieved 100% microprocessor stability across all test cycles, eliminating inductive noise and confirming the technical durability of the hardware layout.

5.2 Scalability, Machine Learning, and IoT Telemetry Expansion

While the 3ft × 2ft prototype successfully confirms the core engineering principles of this design, expanding this system to commercial, multi-acre open-field agricultural installations requires scaling both its mechanical and software frameworks. Future iterations of this work will focus on the following core upgrades:

- **Mechanical Structural Scaling:** Scaling up the canopy assembly to span expansive crop rows will involve replacing the miniature PVC framework with structural aluminum or galvanized steel overhead truss systems. The electromechanical drive will be upgraded to ultra-high-torque industrial NEMA-series stepper motors coupled with planetary gearboxes and heavy-duty steel wire cable pulley tracking mechanisms to maintain structural integrity against high open-field wind shears.
- **Predictive Machine Learning Integration:** The embedded firmware logic will be upgraded from a fixed reactive threshold state machine to a predictive control model. By integrating an array of ambient micro-climate sensors (barometric pressure, relative humidity, ambient temperature, and cloud density photodiodes), an onboard edge-AI processor can run lightweight predictive algorithms to forecast incoming weather fronts and optimize canopy deployment sequences before radiation spikes occur.
- **IoT Cloud Telemetry and Remote Management:** Integrating long-range, low-power communication modules (such as LoRaWAN or Wi-Fi microchip chipsets) will transition the standalone framework into an interconnected Internet of Things (IoT) agricultural network. Building upon earlier environmental impact tracking frameworks like *Ecotracker*, this expansion will enable the system to broadcast real-time micro-climatic data, UV-B levels, motor battery statuses, and canopy tracking diagnostics to a centralized cloud database. Farmers can then monitor field conditions, track daily light integrals, and execute manual overrides through an intuitive mobile or web application dashboard.

Ultimately, this mechatronic canopy system provides a modular, energy-sufficient, and highly scalable foundation for next-generation precision farming, offering a practical solution to preserve crop yields in an increasingly volatile global climate.

IJARSCT
International Journal of Advanced Research in Science, Communication and Technology
International Open-Access, Double-Blind, Peer-Reviewed, Refereed, Multidisciplinary Online Journal
ISSN: 2581-9429
Volume 6, Issue 11, May 2026
Impact Factor: 8.2

REFERENCES

1. R. S. Turner and M. K. Raza, "Stratospheric Ozone Depletion and the Influx of Terrestrial UV-B Radiation: A Comprehensive Review of Agronomic Impacts," *Journal of Environmental Quality and Plant Biology*, vol. 44, no. 3, pp. 211–225, 2024.
2. L. E. Bornman, "Cellular and Molecular Degradation Mechanisms in Crop Canopies Under Accelerated Ultraviolet Stress," *Phytochemical Review Letters*, vol. 18, no. 2, pp. 89–104, 2023.
3. J. M. Given, "The Daily Light Integral (DLI) Conundrum: Balancing Crop Shading with Photosynthetic Efficiency in Protected Agriculture," *IEEE Transactions on Precision Agriculture*, vol. 11, no. 4, pp. 315–328, 2025.
4. A. R. Thakur, "Ecotracker: A Distributed IoT Ecosystem for Multi-Axis Environmental Impact Tracking and Micro-Climate Characterization," *International Journal of Smart Farming Systems*, vol. 7, no. 1, pp. 45–58, 2026.
5. H. Tanaka and S. Mukherjee, "Optoelectronic Isolation and Noise Suppression Paradigms in Low-Voltage Microcontrollers Governing High-Torque Inductive Loads," *Mechatronics and Embedded Automation Systems*, vol. 32, no. 5, pp. 612–624, 2024.